Research Article

Maciej Malicki*, Grzegorz Socha and Józef Krysztofik

Detection of early stage of ductile and fatigue damage presented in Inconel 718 alloy using instrumented indentation technique

https://doi.org/10.1515/eng-2022-0389
received October 07, 2022; accepted November 29, 2022

Abstract: Structural materials under various mechanical loads are damaged as a result of their plastic deformation and subsequent nucleation and propagation of cracks. Detection of damage in its initial phase is crucial to ensure safety and durability of construction elements. In this work, we proposed contact stiffness (S) determined using the instrumented indentation technique as the damage indicator. New procedure for deformation-induced damage investigation is proposed and the indentation tests were performed in the specially designed specimens made from Inconel 718 alloy, which was previously subjected to mechanical loads. Damage parameter (D_ε) determined on the basis of Johnson–Cook damage model was used as a reference measure of damage degree. Fracture analysis was carried out to investigate the early stage of damage development in the tested specimens. The value of contact stiffness determined from the instrumented indentation shows linear correlation with the value of damage parameter. This innovative approach was used in the presented investigation.

Keywords: ductile, fatigue, damage, indentation, hardness, Inconel 718

*** Corresponding author: Maciej Malicki,** Łukasiewicz Research Network – Institute of Aviation, Material and Structure Research Center, Material Testing Laboratory, al. Krakowska 110/114, Warsaw, 02-256, Poland,
e-mail: maciej.malicki@ilot.lukasiewicz.gov.pl
Grzegorz Socha: Łukasiewicz Research Network – Institute of Aviation, Research Coordination Department, al. Krakowska 110/114, Warsaw, 02-256, Polska,
e-mail: grzegorz.socha@ilot.lukasiewicz.gov.pl
Józef Krysztofik: Łukasiewicz Research Network – Institute of Aviation, Material and Structure Research Center, Material Testing Laboratory, al. Krakowska 110/114, Warsaw, 02-256, Poland,
e-mail: józef.krysztofik@ilot.lukasiewicz.gov.pl

1 Introduction

There are a lot of damage mechanisms related to the conditions in which the material is working [1]. In many cases, damage mechanism caused by the mechanical load is related to the plastic deformation of the material. In early development stage, damage takes place at microscopic level and is related to growth of the structure defects in material crystal lattice during plastic deformation. This is manifested at macroscopic level of observation by increase in the hysteresis loop [2,3]. It is commonly accepted that interactions between these structures and the other elements of material structure like grain and phase boundaries correspond to incubation micro cracks and micro voids. Growth and coalescence of this micro discontinuities lead to the formation of dominant crack and final rupture. Incubation of micro discontinuities can take main part of the damage development. That state of affair is especially evident in the case of construction element made from metal alloys which are under cyclic loads. In such cases, the incubation of damage can be responsible for 90% of failure live in the construction element [4–6]. That is why the possibility to detect damage in its early stage is important to ensure the safety and reliability of the constructions. There are many methods to measure the damage introduced into the material. In general such methods rely on measurements of changes in some physical quantity [7–10]. This physical quantity is sometimes called damage indicator. Damage indicators can be divided into categories [7] such as metallurgical, mechanical, physical and parameters related to surface crack quantifications. Most of the mechanical indicators like, for example, strain energy or elastic moduli can be determined only by making specimens from inspected object and laboratory tests. This is serious a disadvantage of such indicators since they cannot be measured for engineering structure under service conditions. On the other hand, such indicators can be the best way to determine progress of damage due to their direct relation with the material ability to carry load.

One of the methods which can be used to measure mechanical properties of material without significantly affecting the element made of this material is the hardness measurements. Use of hardness measurements to determine the material damage has been previously proposed in other publications [8]. In this work indentation tests were used to quantify the damage of Inconel 718 introduced by monotonic and cyclic plastic deformations.

Hardness measurements are performed in small material area which allows one to investigate local changes in the material properties. Since damage process is often limited to a certain volume (especially fatigue damage process), it can be regarded as an additional advantage. In the presented investigation, contact stiffness was used as the damage indicator (S). The reason why we use contact stiffness is the fact that it is related to the indentation modulus E_{IT} [11], which is also a function of Young modulus [12].

$$E_{IT} = (1 - \nu_s^2)\left(\frac{2\beta\sqrt{A}}{S\sqrt{\pi}} - \frac{1 - \nu_i^2}{E_i}\right)^{-1}. \tag{1}$$

Furthermore, Young's modulus is one of the basic mechanical parameters influenced by the material discontinuities [10]. So, E_{IT} should also be influenced by damage progress. Assuming that the Poisson ratio ν_i and elasticity modulus E_i of the indenter material and parameter β related to the shape of the indenter are constant during the measurements, relation between E_{IT} and measured contact stiffness S can be reduced to the formula,

$$E_{IT} \approx \frac{(1 - \nu_s^2)}{1.1284\sqrt{A}}S, \tag{2}$$

where ν_s is the Poisson ratio of the tested material, and A is the projected contact area between the indentation and tested material.

2 Materials and methods

2.1 Materials

The material under investigation is Inconel 718. The chemical composition of this alloy is presented in Table 1. This high-strength and heat-resistant nickel-based alloy is commonly used for components working in the hot sections of rocket and jet engine. One of the reasons of high strength of this alloy is the ability to undergo age hardening process. During this process, fine and hard precipitations of intermetallic γ'' and less significantly γ' phases are formed in the alloy matrix. The structure of the material is typical for annealing process and consists of equiaxed grains with metal carbides (MCs) type primary carbides evenly spaced in the matrix. Recrystallization twins can be seen in Figure 1. The material is not age hardened. It means that the contents of γ'' and γ' are low which makes the material more ductile.

Table 1: Chemical composition of the tested material

C	Mn	P	S	Si	Cr	Ni	Al
0.05	0.01	0.008	0.0002	0.10	17.98	52.30	0.60
Mo	**Cu**	**Nb**	**Ta**	**Ti**	**Co**	**B**	**Fe**
2.88	0.02	4.97	0.01	1.02	0,04	0.002	19.96

2.2 Experimental procedure and design of specimen

For quantifying damage and validating S as a damage indicator, the damage parameter D_ε proposed by Johson–Cook was selected as the reference quantity. D_ε is defined by the formula [13] given by

$$D_\varepsilon = \sum \frac{\Delta\varepsilon}{\varepsilon^f}, \tag{3}$$

where $\Delta\varepsilon$ denotes the increments of the plastic strain intensity during deformation process and ε^f denotes the final value of the accumulated plastic strain intensity corresponding to the failure of the material. This simple definition can be extended to be used in the case of arbitrary deformation along the non-proportional path under complex stress by replacement of the sum of plastic strain intensity increments with the so-called Odqvist's parameter $\bar{\varepsilon}^p$ [14]. In this case, damage indicator is defined as the integral,

$$\Delta\varepsilon = \bar{\varepsilon}^p = \int \mathrm{d}\varepsilon_i^p, \tag{4}$$

where $\mathrm{d}\varepsilon_i^p$ is the infinitesimal increment of plastic strain intensity. Validation of the proposed damage indicators was performed according to the procedure described in the paper [15]. The idea behind this procedure was to produce in single test plastic strain intensity field varying from zero (undamaged state) to that corresponding to the failure, equation (3), in the gage part of the specimen shown in Figure 2. Plastic strain in the gage part cross-sections vary with respect to this cross-section areas and is determined by measuring the geometry of the selected cross-section before and after test, assuming incompressibility of

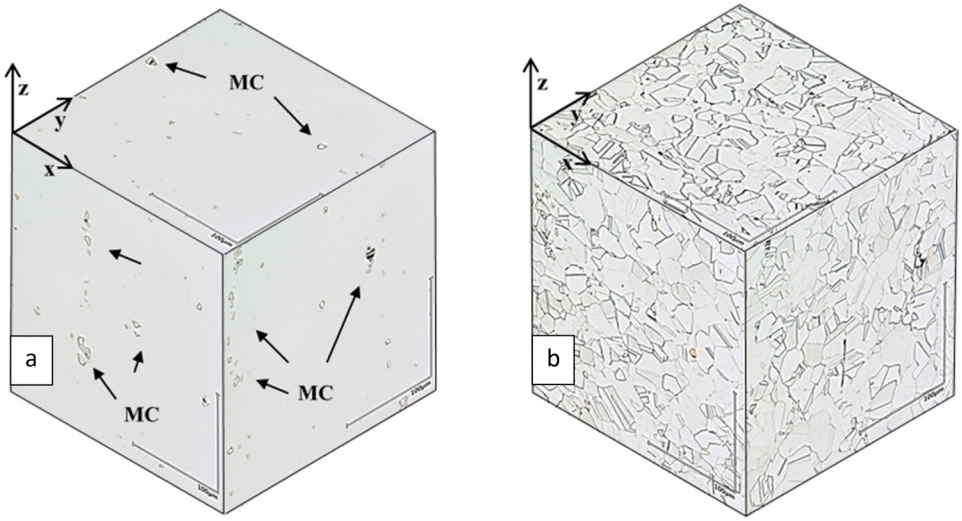

Figure 1: Image of the alloy used in the test. Before (a) and after (b) etching.

the material. Plastic strain intensity in the vicinity of the fractured section is regarded as the failure strain ε^f. Damage parameter as proposed by Johnson–Cook and modified in the paper [16] changes with the progressing accumulation of plastic strain intensity. In the general case of arbitrary loading path in the stress space, it can be used for any mechanism of damage as suggested in the paper [16]. Ratchetting is responsible for damage progress for the applied load scheme, in the case of low cycle fatigue (LCF) and high cycle fatigue (HCF) tests and monotonic deformation in the case of static tension. To verify the usefulness of indentation tests for damage assessment, three specimens as shown in Figure 2 were prepared. If such a specimen is subjected to uniaxial load, non-zero strain tensor components can be identified as principal strains. In terms of principal strain increments, $d\varepsilon_1^p$, $d\varepsilon_2^p$ and $d\varepsilon_3^p$ strain intensity increment $d\varepsilon_i^p$ (see equation (3)) can be expressed by the following formula [17–19]:

$$d\varepsilon_i^p = \sqrt{\frac{2}{9}[(d\varepsilon_1^p - d\varepsilon_2^p)^2 + (d\varepsilon_2^p - d\varepsilon_3^p)^2 + (d\varepsilon_3^p - d\varepsilon_1^p)^2]}. \quad (5)$$

In the case of uniaxial loading along the proportional strain path (simple tension or ratchetting), applying the principle of incompressibility of the material during strain increment

$$d\varepsilon_1{}^p = -(d\varepsilon_2{}^p + d\varepsilon_3{}^p), \quad (6)$$

and for further simplifying the state of strain assuming that

$$d\varepsilon_2{}^p = d\varepsilon_3{}^p = -\frac{1}{2}d\varepsilon_1{}^p. \quad (7)$$

The equations (5) and (4) can be reduced, respectively, to simple formulas as follows:

$$d\varepsilon_i^p = d\varepsilon_1^p, \quad (8)$$

$$\Delta\varepsilon = \bar{\varepsilon}^p = \int d\varepsilon_1^p = \varepsilon_1^p, \quad (9)$$

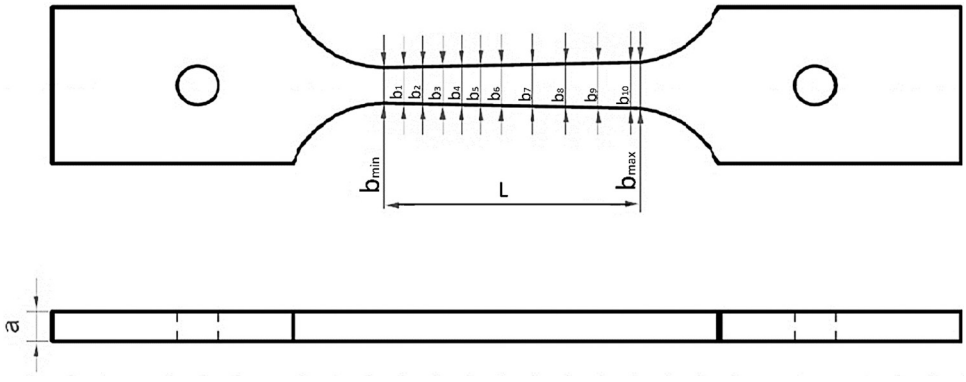

Figure 2: Specimen with varying cross-sections of the gage part used for the investigation.

where ε_1^p is a plastic strain in a direction parallel to the direction of main load applied during the mechanical tests. Reference damage parameter (D_ε) can be now defined as the ratio of plastic strain intensity at a given spot of the material to the value of plastic strain intensity corresponding to the failure of the material using the formula given by

$$D_\varepsilon = \frac{\varepsilon_1^p}{\varepsilon_1^{pf}}. \tag{10}$$

The value of D_ε can be easily calculated on the basis of the measurements of initial and deformed geometry of the specimens gage part cross-sections marked as shown in Figure 2. One of prepared specimens has been subjected to static tensile test at the room temperature (Figure 3a). Testing machine cross-head displacement rate was initially 0.1 mm/min and after reaching strain equal to 0.015 mm/mm, it was increased to 1.2 mm/min and kept constant during the rest of the test till the rupture of the specimen. Damage parameter was calculated using equation (10) for the gage part sections marked in Figure 2. Another two specimens were subjected to oscillating loads (Figure 3b) to introduce the material fatigue damage.

The first specimen was loaded with a maximum stress of 600 MPa at the smallest cross-section of the gage part and cycle asymmetry ratio R = 0.05 (frequency 20 Hz, room temperature) to attain failure at Nf = 125,742 cycles. This corresponds to HCF regime. Second specimen was loaded with a maximum stress of 700 MPa (frequency 20 Hz, room temperature, asymmetry ratio R = 0.05) to rupture at Nf = 60,851 cycles, which corresponds to LCF conditions. For those two specimens, applied stress amplitude for the i-th section of the gage part was lower than that for the smallest cross-section according to the formula (Figure 4) given by

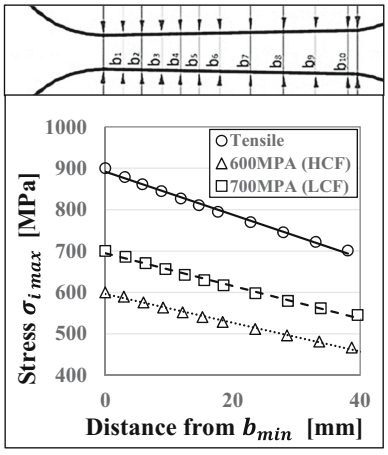

Figure 4: Stress distribution in specimen gage part.

$$\sigma_{i\max} = \frac{b_{\min}}{b_i}\sigma_{\max}, \tag{11}$$

where b_i is the width of the i-th specimen cross-section. Damage in this section corresponds to that introduced by N cycles applied with this amplitude. As mentioned, ratchetting is the main mechanism behind the progress of damage in the case of applied LCF and HCF loading program.

2.3 Equipment used for indentation tests

Indentation tests were performed on a test set-up specially designed and produced for this purpose. This test set-up is shown in Figure 5.

The device is equipped with 2 kN force sensor with a sensitivity of 2.02 mV/V and summary error of measured force ≤0.2% and incremental displacement gauge with

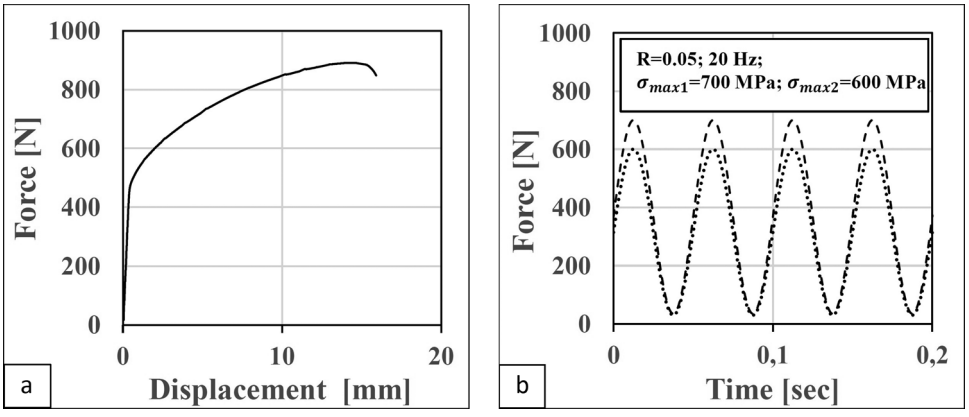

Figure 3: Load scheme for mechanical test performed on speciemns used for the investigation. Tensile test (a) and fatigue test (b).

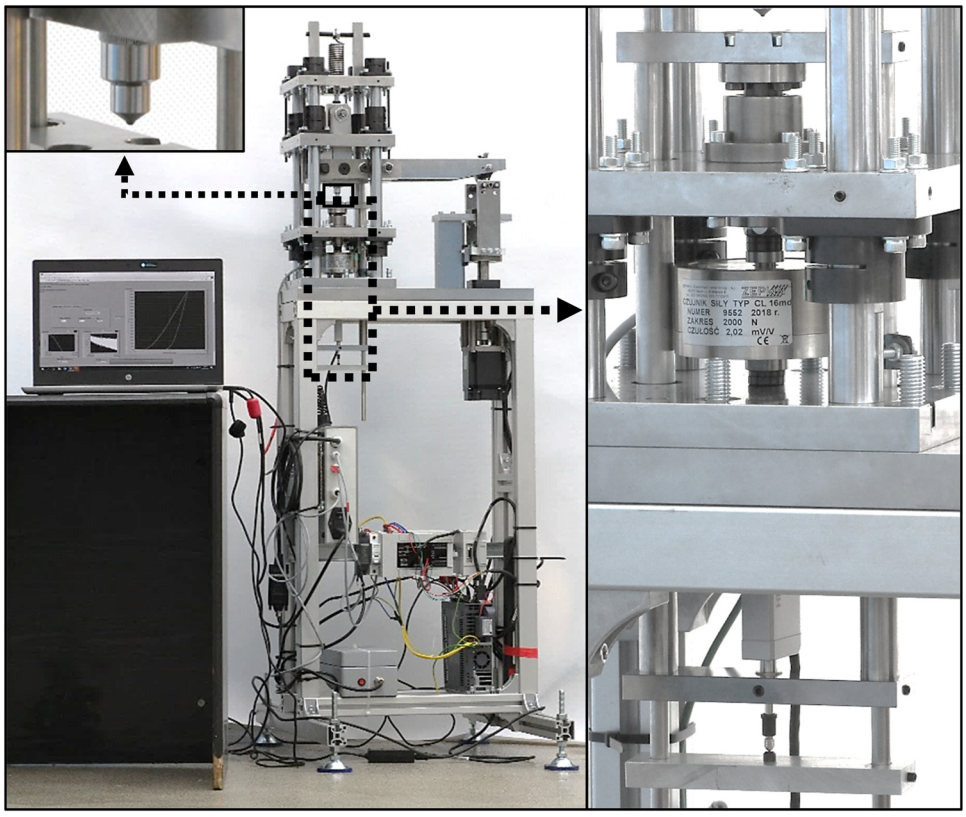

Figure 5: Device for instrumented indentation test.

0.03 µm, typically short-range displacement measurement accuracy. Data from force sensor and displacement gauge were acquired by LabVIEW software using acquisition card with a frequency of 100 Hz and resolution of 0.1 N for force sensor and 0.05 µm for displacement gauge. Tungsten carbide ball with 2.5 mm diameter was used as an intender. The intender was moved by a servo motor. To achieve high positioning accuracy, this move was carried out via a leverage system and ball screw with a diameter of 25 mm and thread pitch of 2 mm. During the indentation tests, displacement (D) of the indenter and acting force (F) were recorded continuously. Test force was limited to 1,600 N. Typical recorded force–displacement plot is shown in Figure 6. Contact stiffness is the slope of the line tangential to the test force removal curve evaluated at maximum test force ($F_{\max}$) [20].

$$S = \left(\frac{\mathrm{d}F}{\mathrm{d}D}\right)_{F_{\max}} = tg(\lambda). \tag{12}$$

Ball size and maximum indentation force have been selected in such a way that the diameter of indentation was greater than at least 100 grains (Figure 7).

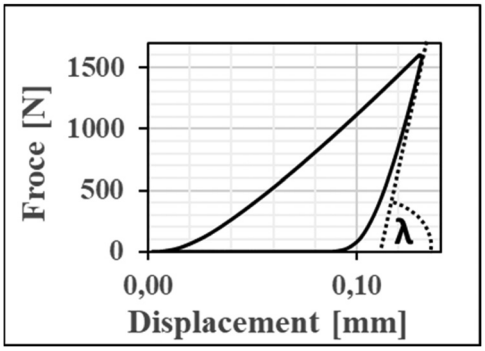

Figure 6: Force–displacement plot from indentation test.

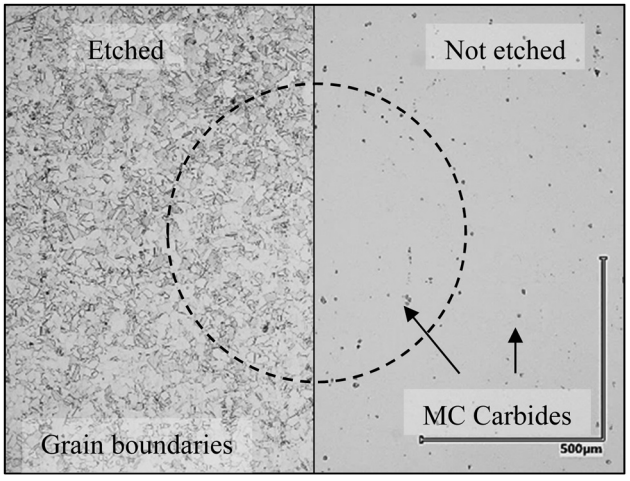

Figure 7: Estimated indentation size with respect to the elements of material structure.

3 Results and discussion

3.1 Damage distribution

For all three kinds of tests (static tension, LCF and HCF) measurement of the width and thickness at marked sections were performed to calculate the plastic strain intensity at the corresponding sections. Using equation (10), the value of damage parameter was calculated and plotted as the function of distance from the ruptured surface (data points correspond to marked sections). Results of the calculations are shown in Figure 8 for all the performed mechanical tests. As it can be seen, value of the damage parameter is the highest for the specimen ruptured under static tension for all the sections of the gage part except fracture surface (where it must be equal to 1 by definition). Also, elongation of the specimen gage part is the highest.

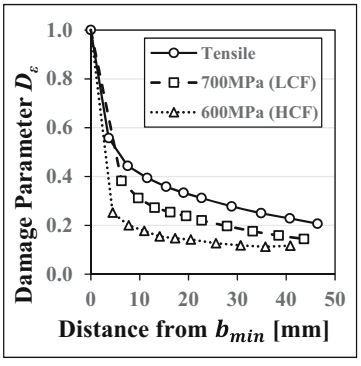

Figure 8: Distribution of the damage parameter in the gage part of the specimens after tests.

The reason for this is the fact that fatigue damage decreases the ability of the alloy to achieve plastic deformation preceding the final rupture of the material. This phenomenon can be attributed to the discontinuities appearing in the material in the form of micro cracks. Their creation and growth limits ratchetting which itself is the result of dislocations formation and their movement in the relatively high material volume (with respect to the size of micro cracks). Such micro-discontinuities grow with the applied load cycles and finally achieve the size enabling triggering of the uncontrolled crack extension leading to final quasi-static rupture of the specimen.

3.2 Fracture analysis

Surface of the specimen's gage part was examined after tests for all three kinds of the applied load program using SEM. Results of the examinations are shown in Figures 9–11. All the images are annotated by the value of the damage parameter calculated according to the procedure described above. As it can be seen, damage of the material at the specimen's gage part surface is run by deformation of the plastic matrix and creation of physical discontinuities at the interface between the matrix and hard inclusions (niobium carbide) due to strain incompatibility. For the fatigue tests, this phenomenon is followed by crack growth (Figures 10 and 11). For all the cases of load, one can see that the progressing damage results in deformation of the material. This deformation is clearly visible, especially in the case of static tension. In the case of fatigue loading, deformation of the surface of gage part can be seen near the neck. For the rest of the gage part, this deformation is hardly visible. This effect can be attributed to the fact that load level comparing to static tension test is much lower and only very localized yielding can be observed.

For the specimen after fatigue test, the fracture surface analysis was performed to define what value of parameter D_ε and contact stiffness S correspond to early stage of fatigue damage. Fracture surfaces are located in the smallest cross-section of specimens. Origin area, fatigue fracture area and final rupture area are visible on the fracture surface of the specimens (Figures 12 and 13). Each of these areas have a different topography. Topography of the origins have crystallographic character which is typical for early stage of fatigue damage development. Origin of the fracture in both the specimens is located in the specimens' surfaces and are about ≥100 μm in width. There is a MC type carbide right in the center of origin of fracture after HCF test (Figure 13b).

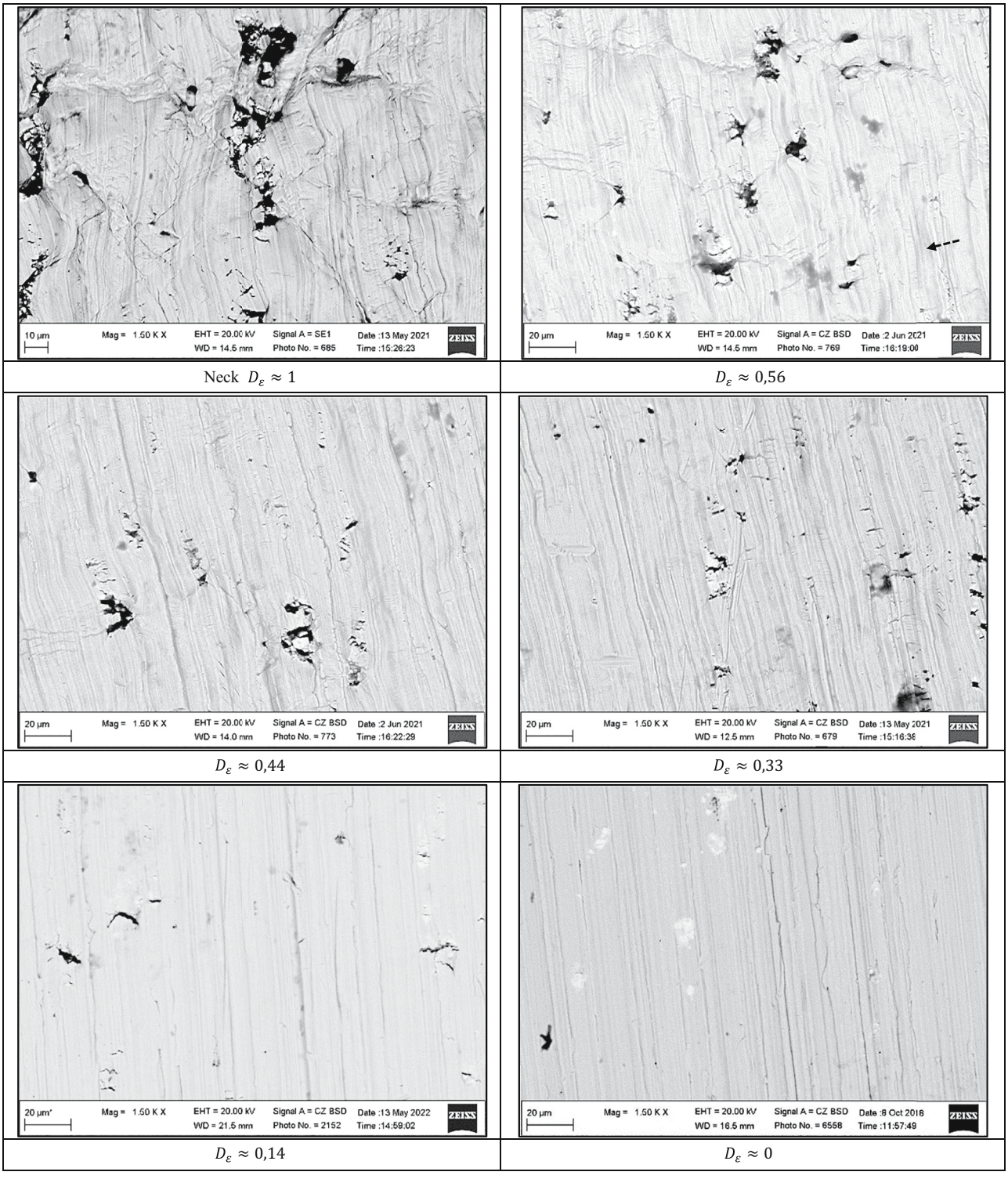

Figure 9: Surface of the gage part – static tension.

In the fatigue area, there are visible fatigue striations which have varying size with respect to the distance from origin. Fatigue areas correspond to the stable fatigue crack propagation. Topography with dimples present in final rupture areas is typical for ductile fracture. These areas correspond to nonstable sudden crack propagation.

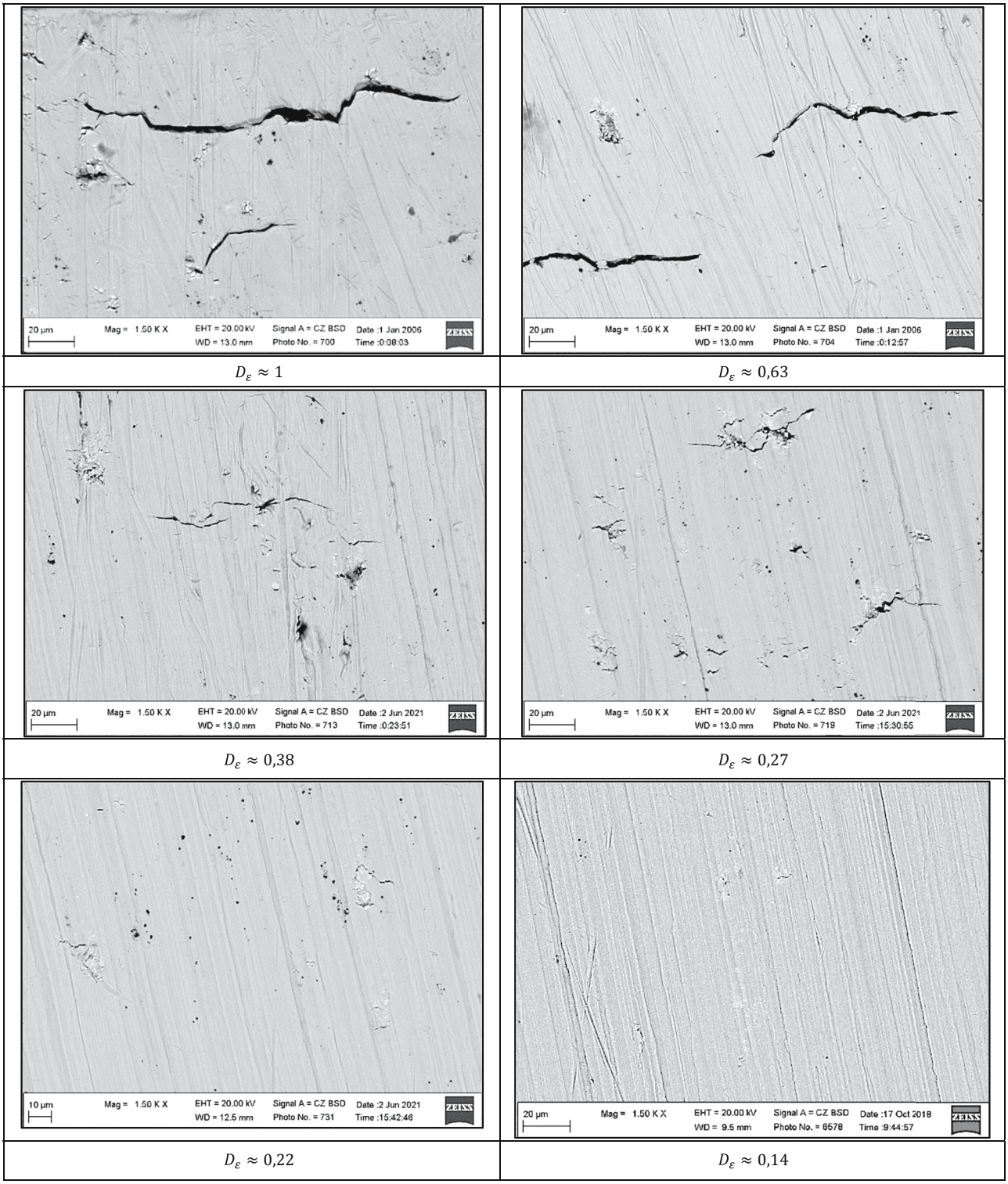

Figure 10: Surface of the gage part – LCF.

Thickness of the striations was measured in different fatigue area for each of the two specimens. The chart presented in Figure 14 is based on these measurements. Curves in this chart represent the approximated crack growth rate function. This function is denoted in Figure 14 as $f(L_{lcf})$ and $f(L_{hcf})$, and its values are simply the

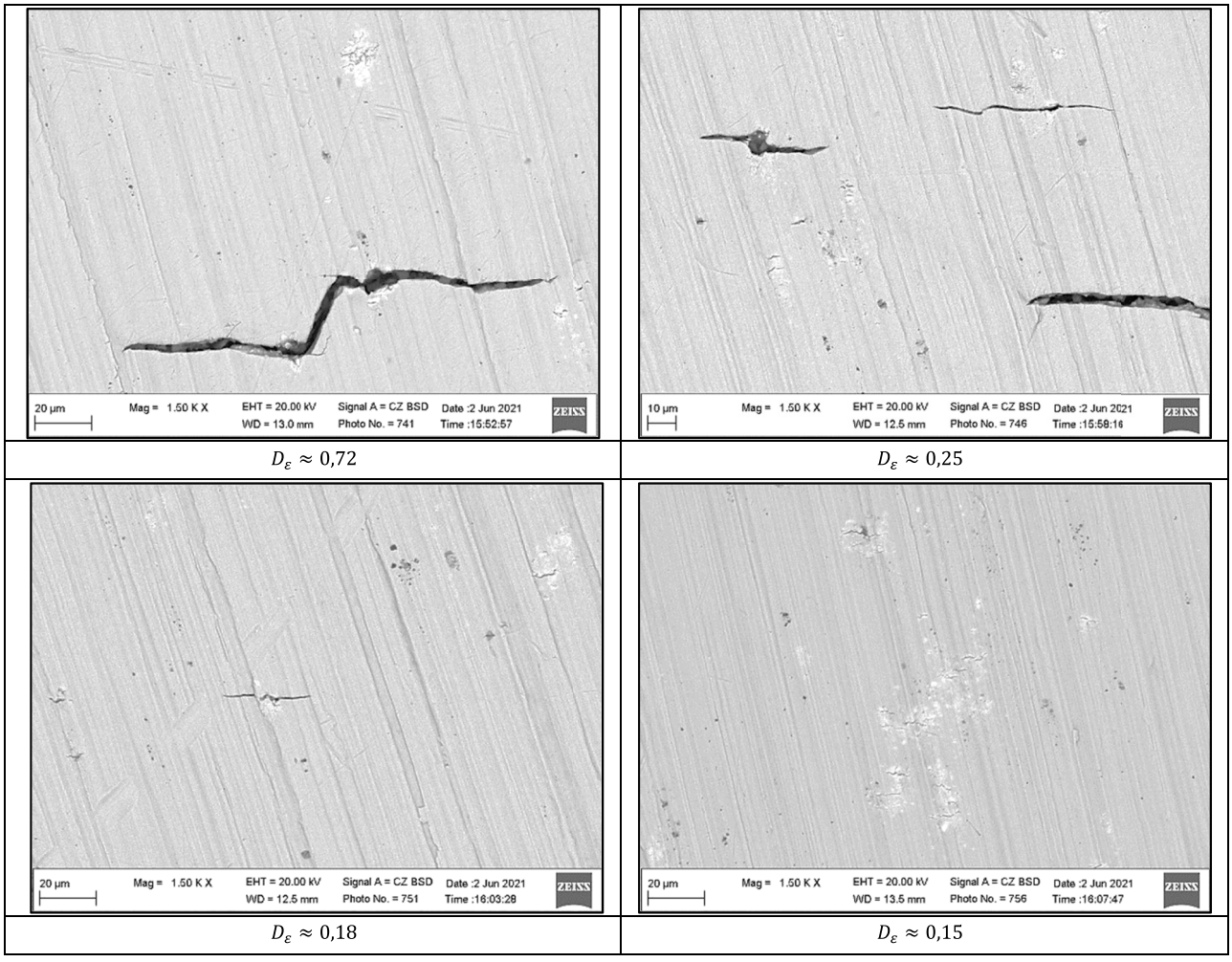

Figure 11: Surface of the gage part – HCF.

thickness of the striations. Using this function and recursive formula (13) (Figure 15) it is possible to estimate the number of load cycles N_{nuclcf} and N_{nuchcf} corresponding to the nucleation of fatigue crack. These estimations showed that approximately 74% (45,000 cycles) of fatigue life for LCF test and approximately 87% (109,000 cycles) of fatigue life for HCF test correspond to the crack incubations phase. For specimen after LCF test, there are cross-sections where the stress level is the same or smaller than in the damage cross-sections of the specimen after HCF. Combining above assumption with the fact that the specimen after LCF test breaks after 60,851 cycles (which is much lesser than the number of cycles needed for incubation of fatigue crack in specimens after HCF test), a conclusion can be drawn.

The conclusion is that in some cross-sections of the specimen, after LCF test, conditions for fatigue damage incubation are satisfied. This cross-section corresponds to the value of damage parameter $D_\varepsilon \leq 0.24$ (Figure 10). For values of damage parameter D_ε ranging from 0.22 to 0.27, there are visible cracks propagating from MC type carbides. Similar source of crack is also visible in areas where D_ε values are higher and damage development is more advance. This indicates that the main mechanism of fatigue damage for LCF and HCF tests is crack propagation and delamination of MC type carbides accompanying ratchetting.

$$L_1 = L_0 - f(L_0),$$
$$L_{n+1} = L_n - f(L_n),$$

If

$$L_{n+1} < 100\ \mu\text{m, then } N_{nuclcf}, \quad N_{nuchcf} = N_f - n, \quad (13)$$

where $f(L_0)$, $f(L_1)$, $f(L_n)$ and $f(L_{n+1})$, are the values of functions $f(L_{lcf})$ and $f(hcf)$ calculated for crack length L_0, L_1, L_n, L_{n+1}, respectively, and N_f is the number of cycles to attain failure.

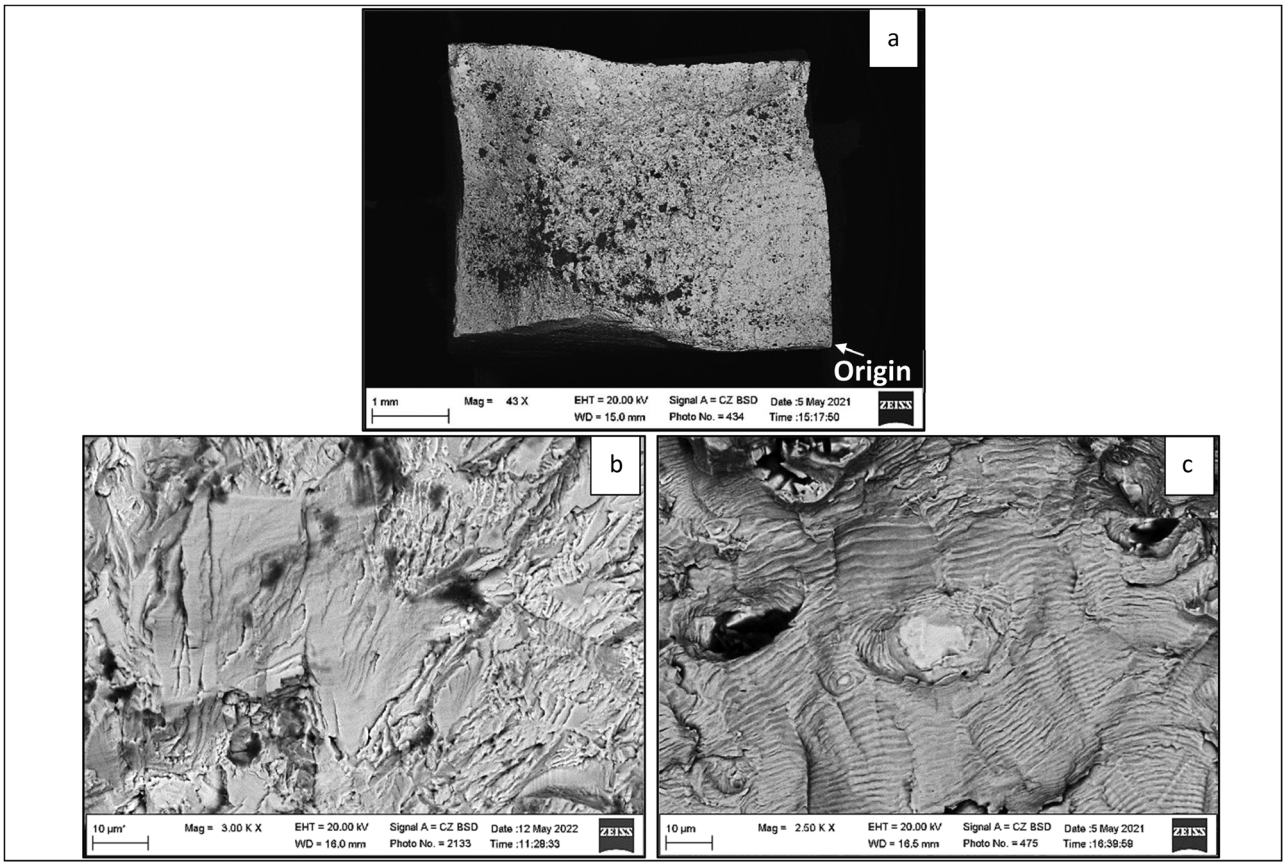

Figure 12: Fracture surface (a), origin area (b) and fatigue zone (c) of the specimen after LCF test.

3.3 Contact stiffness

Based on the indentation measurement performed on the tested specimens, contact stiffness (S) determined from equation (12) decreases with the increase in the damage parameter (Figure 16). Such a tendency is also maintained for the early stage of damage developed in specimen after LCF test, which was defined before with respect to the values of damage parameter ($D_\varepsilon \leq 0.24$, green area in Figure 16). However, contact stiffness determined from equation (12) does not refer only to the properties of the specimen material but also to the frame stiffness and in general case is a total stiffness (S_{tot}). Total stiffness can be described as inversion of the sum of the frame compliance (C_{fr}) and the inverse of stiffness related to specimen (S_{spec}) [21] (formula (13) and Figure 17).

$$S_{\text{tot}} = \left(C_{\text{fr}} + \frac{1}{S_{\text{spec}}}\right)^{-1} = \left(C_{\text{const}} + C_{\text{indent}} + \frac{1}{S_{\text{spec}}}\right)^{-1}. \quad (14)$$

Moreover, frame compliance can be taken as a sum of constant compliance component (C_{const}) of machine frame and indentation compliance (C_{indent}) which vary depending on the depth of the indentation. The main task in our investigations is to find the changes in contact stiffness related to the material damage and so we can disregard the value of S_{spec}. That is why the C_{const} component of the frame compliance can be neglected assuming that it is the same for all indentation measurements. Using this assumption and formula (13), the relative specimens stiffness S'_{spec} can be introduce and simply described by equation:

$$S'_{\text{spec}} = \left(\frac{1}{S_{\text{tot}}} - C_{\text{indent}}\right)^{-1}. \quad (15)$$

Based on the investigations presented in paper [21], the C_{indent} can be expressed by the equation as follows:

$$C_{\text{indent}} = \frac{1}{E\pi 2R}\ln\left(\frac{l}{(2R - l)}\left(\frac{2R}{h_c} - 1\right)\right), \quad (16)$$

where E is the modulus of elasticity of indenter material, R is the radius of the intender, l is the total height of the indentation, h_c is the indentation depth. Using equations (15) and (16), the stiffness related with the specimen can be expressed by the formula as follows:

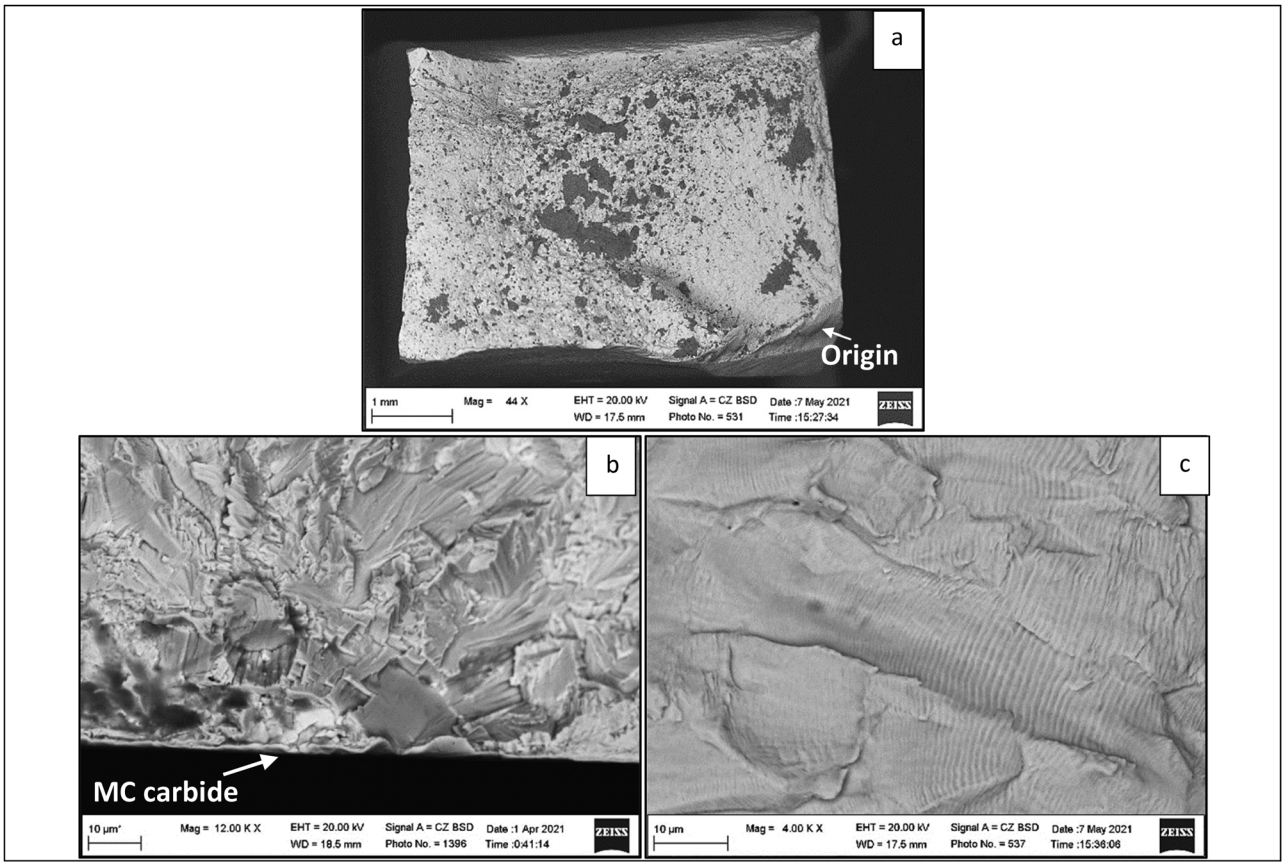

Figure 13: Fracture surface (a), origin area (b) and fatigue zone (c) of the specimen after HCF test.

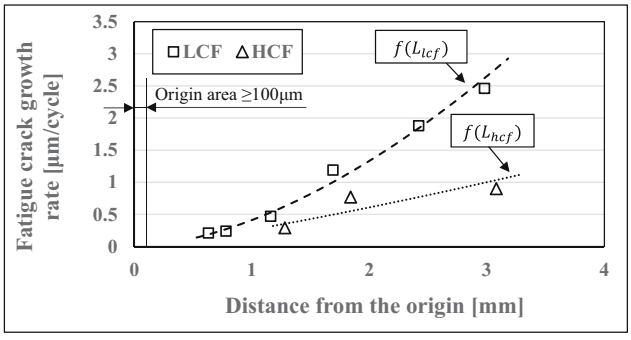

Figure 14: Chart representing the fatigue crack growth rate for specimens after LCF and HCF tests.

$$S'_{\text{spec}} = \left(\frac{1}{S_{\text{tot}}} - \frac{1}{E\pi 2R} \ln\left(\frac{l}{(2R - l)\left(\frac{2R}{h_c} - 1 \right)} \right) \right)^{-1}. \quad (17)$$

According to this equation, the highest impact of C_{indent} on changes in the total contact stiffness is for indentations with relatively small depth where greater part of the indenter is not involved in their creation (Figure 18). Indentations made in the tested specimens have depth in the range from 0.060 to 0.094 mm. That means changes in C_{indent} are in the range from 9.09×10^{-7} to 7.94×10^{-7} mm/N (Figure 18).

The impact of C_{indent} on the contact stiffness of S'_{spec} is manifested by the increase in its values with respect to the values of S_{tot} (Figure 19). The impact of contact stiffness changing tendency with respect to the damage parameter is insignificant. In the measuring machine displacement measurement system was based on a surface of measuring table. This means that on the value of specimen stiffness will have impact not only the volume related with indentation but also volume of the material behind indentation area.

This is another source of measuring bias due to variation in specimen thickness inducted by plastic deformation which are results of earlier performed tensile and fatigue tests. This bias can be estimated and reduced using the finite element analysis and selection of the base for displacement measurement. To estimate the specimen thickness effect on the determined contact

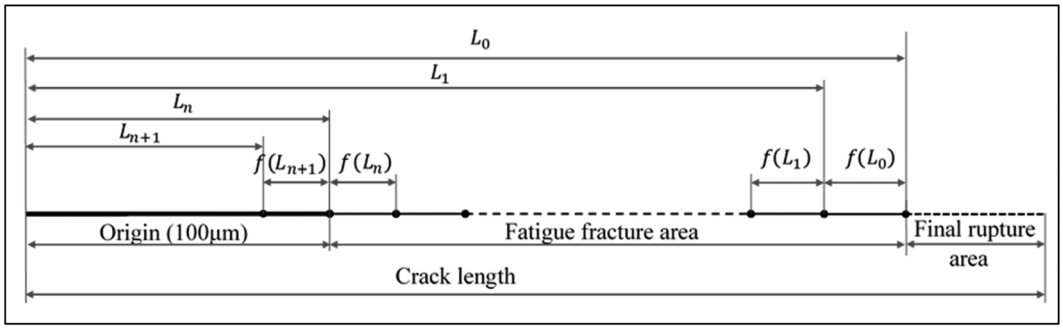

Figure 15: Diagram of notation used in the recursive formula (10).

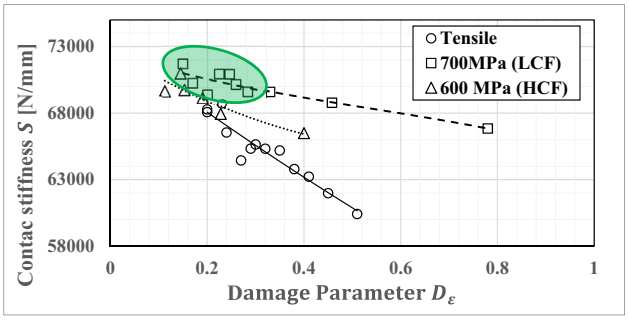

Figure 16: Results of contact stiffness measured for specimens after tensile test and fatigue test in areas with different values of damage parameter D_ε.

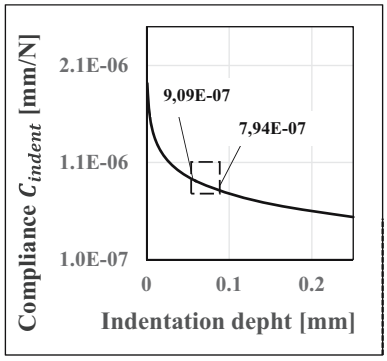

Figure 18: Estimated changes (using equation (16)) in compliance C_{indent} with respect to the indentation depth for ball indenter with 2.5 mm diameter made from tungsten carbides.

stiffness, the modification of displacement measured system was made. After this modification, the base of the displacement measurement was upper specimen surface. It was found that contact stiffness S_{tot} measured on modified set-up for undamaged tested material is ≈20% higher than in the previous one (Figure 20). It means that reduction in specimen thickness caused by specimen deformation during mechanical tests has the influence on changes in S'_{spec} depending on the damage parameter presented in Figure 19.

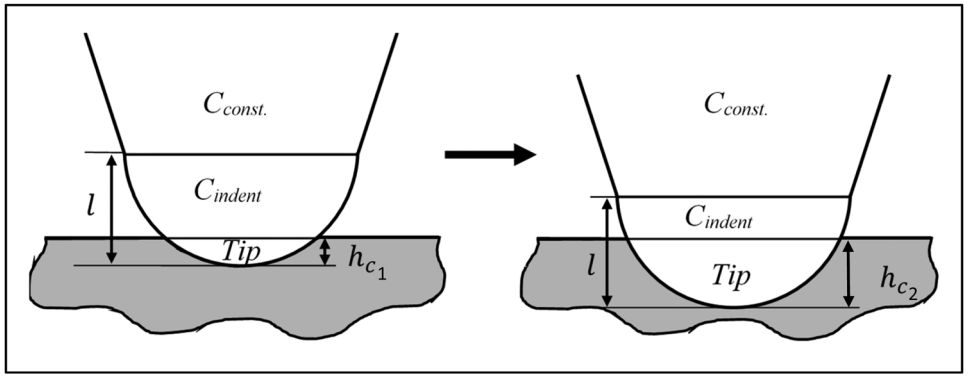

Figure 17: Illustration of machine frame contact stiffness components.

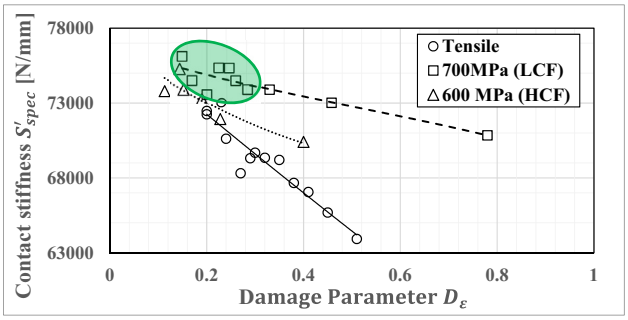

Figure 19: Results of contact stiffness measured for specimens after tensile test and fatigue test in areas with different values of damage parameter D_ε. As shown in Figure 16, green area correspond to early stage of damage developed in specimen after LCF test.

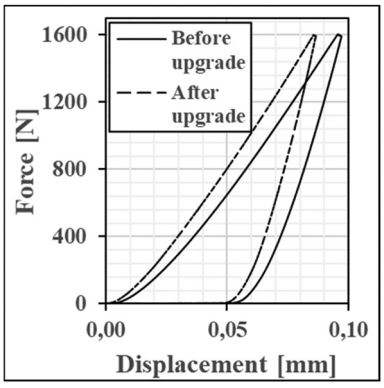

Figure 20: Force–displacement plot from indentation test before and after modification of displacement measuring system.

4 Conclusion

Damage introduced into the tested material by conducted mechanical tests results in changes in the selected damage indicator. Damage of the material was quantified by reference damage parameter proposed by Johnson–Cook. Analysis of investigation results leads to the following conclusions:

1. Damage process in the case of static tension of Inconel 718 is run by increased density of dislocations, their movement and nucleation and growth of micro-discontinuities at the interface between the ductile matrix and hard inclusions (niobium carbide). Occurrence of all these phenomena was found at an early and late stage of damage development.
2. Damage process in the case of cyclically loaded Inconel 718 is run by nucleation and growth of micro cracks which is accompanied by the ratchetting phenomenon.
3. It has been found that the measured contact stiffness decreases during the increase in damage parameter D_ε. The tendency of these changes is the same for early and later stage of damage development.
4. Using displacement measurement system based on the specimen upper surface is a possible way for the development of the proposed technique for measured contact stiffness
5. In the future work, it is possible to simulate the force–displacement curves obtained from instrumented indentation by using a phenomenological approach using models that can be found in the literature [22]. It is also possible to evaluate elastoplastic properties of the material (including elastic modulus, yield strength and strain hardening exponent) from these curves [23–25].

Conflict of interest: Authors state no conflict of interest.

References

[1] ASM Handbook. In: Becker WT, Shipley RJ, editors. Failure Anaysis and Prevention. Vol. 11. edition 2002. Eight printing November 2014.
[2] Vaiana N, Sessa S, Marmo F, Rosati L. A class of uniaxial phenomenological models for simulating hysteretic phenomena in rate-independent mechanical systems and materials. Nonlinear Dyn. 2018;93:1647–69. Springer. doi: 10.1007/s11071-018-4282-2.
[3] Vaina N, Sessa S, Rosati L. A generalized class of uniaxial rate-independent models for simulating asymmetric mechanical hysteresis phenomena. Mech Syst Signal Process. 2021;146:106984. doi: 10.1016/j.ymssp.2020.106984.
[4] Kowalewski ZL. Zmęczenie materiałów -podstawy, kierunki badań, ocean stanu uszkodzenia Siedemnaste seminarium nieniszczące badania materiałów. Zakopane 8-11 marca; 2011.
[5] Kocańda S. "Zmęczeniowe niszczenie metali" WNT; 1978.
[6] Davidson D, Chan K, McClung R, Hudak S. Comprehensive Structural Integrity. Vol. 45; 2003. p. 129–64.
[7] Yang L, Fetami A. Cumulative fatigue damage mechanisms and quantifying parameters: A literature review. J Test Eval. March 1998;26(2):89–100.
[8] Gorkunov ES, Smirnov SV, Rodionowa SS. Influence of plastic deformation at hydrostatic pressure on damage and magnetic characteristics of low-carbon steel 3sp. Phys Mesomech. 2003;6(5):101–8.
[9] Socha G. Experimental investigations of fatigue cracks nucleation, growth and coalescence in structural steel. Int J Fatigue. 2003;25(2):139–47.
[10] Lemaitre J. A course on Damage Mechanics. Berlin Heidelberg: Springer-Verlag; 1996.
[11] Hay JL, Pharr GM. Instrumented Indentation Testing. 2000 ASM International. Handbook. Vol. 8. Mechanical Testing and Evaluation (#06772G).
[12] PN EN ISO 14577-1:2015 Metallic materials – Instrumented indentation test for hardness and materials parameters- Part 1: Test method; 2015.

[13] Johnson GR. Materials characterization for computations involving severe dynamic loading. Proc. Army Symp. Of Solid Mechanics. Cape Cod, Mass; 1980. p. 62–7.
[14] Odqvist FKG. Die Verfestigung von flusseisenaehlichen Koerpern. ZAMM. 1933;13(5):360–3.
[15] Socha G, Madejski B, Malicki M. Study on deformation-induced damage evolution for Inconel 718 super alloy with the use of an innovative single-specimen method. J Theor Appl Mech. 2016;54(4):1379–90.
[16] Socha G. Fatigue damage indicators based on plastic deformation. ASTM Special Technical Publication. 2017;246–57. Volume STP 1598.
[17] Johnson GR, Cook WH. Fracture characteristic of three metals subjected to various strains, strain rate, temperatures and pressures. Eng Fract Mech. 1985;21(1):31–48.
[18] Hancock JW, Mackenzie AC. On the mechanisms of ductile failure in high-strength steels subjected to multi-axial stress-states. J Mech Phys Solids. 1976;24:147–69. Pergamon Press
[19] Paulo Davim J. Introduction to mechanical engineering. Cham: Springer; 2018. ISBN 978-3-319-78487-8. p. 19.
[20] Olivier WC, Pharr GM. Measurement of hardness and elastic modulus by instrumented indentation: Advances in understanding and refinements to methodology. J Mater Res. Jan 2004;19(1):3–20. doi: 10.1557/jmr.2004.0002.
[21] Kang SK, Kim JY, Kang I, Kwon D. Effective indenter radius and frame compliance in instrumented indentation testing using a spherical indenter. J Mater Res. Sep 2009;24(9):2965–73.
[22] Vaiana N, Rosati L. Classification and unified phenomenological modeling of complex uniaxial rate-independent hysteretic responses. Mech Syst Signal Process. 2023;182:109539. doi: 10.1016/j.ymssp.2022.109539.
[23] Lee JH, Kim T, Lee H. A study on robust indentation techniques to evaluate elastic–plastic properties of metals. Int J Solids Struct. 2010;47:647–64. doi: 10.1016/j.ijsolstr.2009.11.003.
[24] Kucharski S, Mróz Z. Identification of material parameters by means of compliance moduli in spherical indentation test. Mater Sci Eng A. 2004;379:448–56. doi: 10.1016/j.msea.2004.03.030.
[25] Kim M, Marimuthu KP, Lee JH, Lee H. Spherical indentation method to evaluate material properties of high-strength materials. Int J Mech Sci. 2016;106:117–27. doi: 10.1016/j.ijmecsci.2015.12.008.